Reaction Engineering Implications of Cellulose Crystallinity and Water-Promoted Recrystallization

Maksim Tyufekchiev[a], Alex Kolodziejczak[a], Pu Duan[c], Marcus Foston[b], Klaus Schmidt-Rohr[c], Michael T. Timko[a]

[a] Department of Chemical Engineering, Worcester Polytechnic Institute, 100 Institute Road, Worcester, MA, 01609, USA

[b] Department of Energy, Environment and Chemical Engineering, Washington University in St. Louis, One Brookings Drive, St. Louis, MO 63130, USA

[c] Department of Chemistry, Brandeis University, 415 South Street, Waltham, MA 02453, USA

Abstract.

Mechanical decrystallization and water-promoted recrystallization of cellulose were studied to understand the effects of cellulose crystallinity on reaction engineering models of its acid-catalyzed hydrolysis. Microcrystalline cellulose was ball-milled for different periods of time, which decreases its crystallinity and increases the glucose yield obtained from acid hydrolysis treatment. Crystallinity increased after acid hydrolysis treatment, which has previously been explained in terms of rapid hydrolysis of amorphous cellulose, despite conflicting evidence of solvent promoted recrystallization. To elucidate the mechanism, decrystallized samples were subjected to various non-hydrolyzing treatments involving water exposure. Interestingly, all non-hydrolyzing hydrothermal treatments resulted in recovery of crystallinity, including a treatment consisting of heat-up and quenching that was selected as a way to estimate the crystallinity at the onset of hydrolysis. Therefore, the proposed mechanism involving rapid hydrolysis of amorphous cellulose must be incomplete, since the recrystallization rate of amorphous cellulose is greater than the hydrolysis rate. Several techniques (solid-state nuclear magnetic resonance, X-ray diffraction,

and Raman spectroscopy) were used to establish that water contact promotes conversion of amorphous cellulose to a mixture of crystalline cellulose I and cellulose II. Crystallite size may also be reduced by the decrystallization-recrystallization treatment. Ethanolysis was used to confirm that the reactivity of the cellulose I/cellulose II mixture is distinct from that of truly amorphous cellulose. These results strongly point to a revised, more realistic model of hydrolysis of mechanically decrystallized cellulose, involving recrystallization and hydrolysis of the cellulose I/cellulose II mixture.

1. Introduction

Cellulose is an abundant and renewable source of carbon with potential to serve as a feedstock for the production of fuels and chemicals.[1-3] In addition, due to its physicochemical properties cellulose finds high value applications in the polymer, pharmaceutical, and nanomaterial fields.[4-6] Depolymerization of cellulose using hydrolysis and other methods is deemed essential for economical production of lignocellulose-based products and accordingly it has received attention as a research area for decades.[5, 7-9] Various approaches have been studied to depolymerize cellulose to monosaccharides that can be converted and upgraded to fuels and chemicals. One of the most promising routes involves cellulose hydrolysis to glucose.[7, 10-16] However, cellulose, particularly cellulose that is part of lignocellulosic biomass, exhibits low chemical and biological reactivity, making necessary severe conditions, excess biocatalysts, and energy intensive pretreatments to break down its structure.[8, 14, 17-22] As a result, cellulose depolymerization remains a technological and economic bottleneck for commercialization of otherwise promising second generation biofuel technologies, including cellulosic bioethanol.[9, 23]

Cellulose depolymerization approaches are either energy intensive, slow, or result in degradation of valuable products.[24-27] To identify approaches that increase cellulose reactivity,

many studies have investigated the relationships between cellulose's reactivity and its polymer structure.[28-30] Cellulose reactivity has been attributed to many different physico-chemical structural characteristics, including the chemical composition of the lignocellulosic complex itself;[29] the interconnectedness of lignin, hemicellulose, and cellulose;[31, 32] cellulose particle size,[33, 34] surface area,[30, 34] pore structure,[34, 35] degree of polymerization,[34] accessibility,[34, 36] and especially crystallinity,[28-30, 37-41] i.e., the relative amount of crystalline and amorphous regions present in the cellulose. In particular, decrystallization of cellulose has been reported to increase the cellulose conversion rate, an empirical observation that implies that crystallinity is important to cellulose recalcitrance.[28, 30, 37, 38, 42-44]

Observations of decreasing hydrolysis rates with increasing conversion have motivated the development of qualitative and quantitative models with separate reaction rates for amorphous and crystalline cellulose.[45] Kinetic models that explicitly relate cellulose reactivity to its crystallinity date back to at least 1947 when Philipp et al.[45] proposed a two parameter amorphous-crystalline cellulose hydrolysis model to fit rate data obtained from acid-catalyzed cellulose solubilization. In the Philipp et al.[45] model, the first order rate constant for amorphous cellulose hydrolysis (k_a) is an order of magnitude greater than that for hydrolysis of crystalline domains (k_c). Following its introduction, the theory of differential reactivity of amorphous and crystalline regions has been used to explain numerous experimental results, especially the observation of increased cellulose conversion and glucose yield associated with decreasing cellulose crystallinity.[11, 28, 30, 38, 42, 43, 46-50] The differential reactivity model has similarly been used to explain the observation that cellulose crystallinity increases after hydrolytic treatment, an observation which has typically been attributed to preferential removal of the supposedly more reactive amorphous regions during hydrolysis, one of the key predictions of the theory.[38, 42, 51, 52]

Reaction engineering models that include explicit differences in the reactivity of crystalline and amorphous cellulose are confounded by the fact that exposure of decrystallized cellulose to liquid water or water vapor promotes recrystallization, even under non-hydrolyzing conditions.[53-56] Even though the molecular-level details of this re-structuring are not fully understood, the phenomenon itself is empirically well established, having been reported several times previously by investigators using different characterization techniques.[57-61] Despite the fact that many cellulose depolymerization techniques involve a liquid or vapor water phase,[8, 38, 60, 62, 63] cellulose hydrolysis models do not account for a water-promoted cellulose recrystallization pathway. In fact, correlations between crystallinity and reactivity are based on crystallinity measured prior to sample exposure to the aqueous conditions of hydrolysis.[28, 38, 40, 43, 64] Considering the fact that decrystallized cellulose recrystallizes on contact with water, the actual crystallinity of the sample undergoing hydrolysis is not clear. As a result, the common observation that cellulose crystallinity increases after water-based conversion processes[38, 40, 42] might plausibly be due in part – or in total – to non-hydrolytic recrystallization,[60] placing in doubt one of the core pieces of supporting evidence used for the differential reactivity theory. These considerations point to a gap in the current understanding of cellulose hydrolysis reaction mechanisms, even at the most qualitative level of determining which steps are required for a physically meaningful mechanism.

The objective of this work was to determine the effect of water-induced recrystallization on cellulose reactivity and provide fundamental understanding of the relevant physical and chemical phenomena that occur during hydrolysis. To do so, we ball-milled microcrystalline cellulose for different durations and quantified the relative crystallinity of the resulting samples using X-ray diffraction (XRD). We then subjected these samples to hydrolysis treatment to reproduce literature results and replicate a correlation between measured crystallinity and

reactivity commonly reported in the literature.[28, 38, 40, 42] Next, these same samples were subjected to water-induced recrystallization under non-hydrolytic conditions to examine the effect of water exposure on crystallinity and attempt to measure the crystallinity of the samples at the onset of hydrolysis. Raman spectroscopy was used to provide support for XRD data and expand molecular-level understanding. Solid-state ^{13}C nuclear magnetic resonance (ssNMR) was applied to distinguish cellulose I, cellulose II, non-crystalline chains on the crystallite surface, and truly amorphous cellulose. Through spectral editing based on spin–lattice relaxation, peaks of cellulose I and II could be separated from overlapping non-crystalline bands and quantified fairly accurately.[65] Finally, reactivity under ethanolysis conditions was evaluated in an attempt to differentiate the reactivity of recrystallized cellulose from amorphous cellulose. These results guide the development of quantitative and predictive cellulose hydrolysis reaction engineering models and provide new motivation for developing methods of overcoming the challenge of cellulose recalcitrance.

2. Methodology

2.1 Materials.

Avicel PH101 cellulose (average particle size of 50 μm, 100% purity with 3-5% moisture content), 0.1 M hydrochloric acid standard, cellobiose >98%, glucose >99.5% , hydroxymethyl furfural (HMF) >99% purity, levulinic acid >98%, formic acid >98%, were purchased form Sigma Aldrich. Acetone and ethanol ACS grade were purchased from Pharmco-Aaper. All chemicals were used as received.

2.2 Ball-milling.

Microcrystalline cellulose (MCC) was ball-milled for different durations to generate a family of samples with varying degrees of crystallinity. Briefly, 1.0 gram of MCC was placed in a

stainless steel cylinder (18 mm diameter×55.5 mm length, 10 mL). Three stainless steel balls (2×9.5 mm diameter and 1×15.85 mm diameter) were placed in the cylinder. The cylinder was clamped within the holder of a vibratory shaker Retsch MM2000 and samples were ball milled for 10, 20, 30, 40, and 50 minutes. The temperature was not controlled during milling. The initial temperature is the same as ambient (22-26 °C). Temperature increases during treatment, rapidly reaching a maximum of 50-60 °C after several minutes. This temperature appears to be a steady state between frictional heating and ambient loss.

2.3 Acid Hydrolysis.

Cellulose samples were depolymerized using hydrochloric acid to determine the relationship between cellulose structure and reactivity. Acid treatment conditions were as follows: 0.25 g of cellulose, 5.0 mL of 0.1 M HCl, and a magnetic stir bar were added to a 15 mL heavy wall pressure vial sealed by a screw cap with a Viton O-ring seal. The vial was submerged in an oil bath to heat the reaction mixture to 150 °C, as measured by a thermocouple inserted directly into the reaction mixture through a modified screw cap. The reaction mixture was stirred at 200 rpm for the duration of the reaction time. After the desired reaction time, the vial was removed from the oil bath and quenched in cold water. The reactor vials were centrifuged at 1400 rpm for 15 minutes, and the supernatant liquid was extracted with a syringe for further analysis. After removal of the supernatant liquid, the solids were washed with acetone to remove any residual water. The samples were centrifuged and the acetone was removed by syringe and the remaining solids were transferred into a pre-weighed crucible. The crucible containing the solid product was covered and placed in an oven held at 65 °C until the weight stops changing. The total amount of residual solids was determined gravimetrically.

Concentrations of water soluble products were determined by HPLC analysis of the liquid recovered from centrifugation. The glucose yield was calculated based on the following formula: $\frac{m_g * M_{gu}}{m_c * M_g} * 100\%$, where m_c is mass of cellulose, m_g is mass of glucose determined by HPLC, M_{gu} is molecular weight of glucose unit in cellulose, and M_g is molecular weight of glucose. All experiments were carried out at least in triplicate. Error bars are reported as the standard deviation of replicated experiments.

2.4 Hot Liquid Water Treatment.

Cellulose samples were treated in hot liquid water to determine the effect of the treatment on the structure of cellulose and to determine the glucose yield under conditions lacking acid. The hydrothermal, hot liquid water treatment was identical to the acid treatment described previously, with the exception that no HCl was added to the reaction mixture.

2.5 Recrystallization Tests.

To test whether recrystallization in hot liquid water conditions recovers recalcitrance, cellulose was ball milled for 50 minutes as described before. The ball-milled cellulose (0.50 grams) and 5.0 mL of water were placed in high-pressure glass reactor vials, which were then placed in a preheated oil bath. The treatment was carried out at three different temperatures of 110 °C, 130 °C, and 150 °C. The treated cellulose was recovered and dried as described before. Following the treatment, the cellulose samples (0.25 grams) were hydrolysed by 0.1 M HCl (5.0 mL) for one hour at 150 °C reaction temperature, again as described previously. The liquid sample was extracted and analyzed using HPLC.

2.6 Liquid Product Analysis and Quantification.

The liquid products obtained from both acid and liquid hot water treatments of cellulose were analyzed for water-soluble compounds using High Performance Liquid Chromatography

(HPLC, Agilent 1200 series). A diode array detector (DAD) was used for organic acids and furanic compounds and a refractive index detector (RID) for carbohydrate detection. The column was a Bio-Rad Aminex HPX-87H; the mobile phase was 5 mM sulfuric acid; and the mobile phase flowrate was 0.6 mL min^{-1}. The column and the RID detector were both kept at 35 °C during analytical runs, while the UV-Vis detection wavelength was set to 284 nm. Calibration curves were determined from analysis of mixtures containing known concentrations of standards at 0.25, 0.5, 0.75, 1, 1.25, 1.5, 1.75, 2, and 2.5 g L^{-1}.

2.7 X-Ray Diffraction (XRD).

X-Ray diffraction (XRD) analysis was carried out with Rigaku Geigerflex diffractometer using CuKα radiation at 37.5 kV and 25 mA. A step size of 0.05° was used with 1 second accumulation time. Diffractograms of different samples were compared after area normalization and baseline subtraction. Crystallinity index was calculated by the widely used method first developed by Segal.[66] In this method, the crystalline contribution is determined by the intensity of the 002 peak at 22.5° and the amorphous by the intensity at 18.3°.[66] Crystallinity index was calculated based on the following equation $CI = \frac{I_{200} - I_A}{I_{200}} * 100\%$.

2.8 Raman Microscopy.

Raman spectral analysis of cellulose samples was carried out with a Horiba Xplora Raman Microscope using 785 nm excitation laser and 10× Olympus magnification lens.

2.9 Solid-state Nuclear Magnetic Resonance (ssNMR).

NMR experiments were performed using a Bruker DSX400 spectrometer operating at a ^{13}C resonance frequency of 100 MHz, using a 4-mm magic-angle spinning probe in double-resonance mode at a spinning frequency of 9 kHz and at room temperature. The ^{13}C chemical shifts were externally referenced on the neat TMS scale using the carboxyl peak of α-glycine at 176.49 ppm.

Typical 90° pulse lengths were 3.6 μs for ^{1}H and 4 μs for ^{13}C. MultiCP[67] with composite-pulse excitation and storage[68] was used to obtain nearly quantitative ^{13}C spectra. Five blocks of CP were implemented with 90–100% amplitude ramps on the ^{1}H channel. The contact time for each CP period was 1.1 ms, resulting in a total combined CP contact time of 5.5 ms. The delays for ^{1}H repolarization were 4 s for all samples, while the recycle delay was 8 s. A rotation-synchronized Hahn spin echo[69] was used to achieve dead-time-free detection, generated by a 180° pulse with EXORCYCLE[70] phase cycling after the last multiCP block. During the 18.7-ms detection, proton decoupling with the SPINAL64 scheme[71] was applied, at a ^{1}H strength of $\nu_1 \approx 85$ kHz. The number of scans averaged was 512 for MCC, 1280 for MCC-BM50, 768 for MCC-BM50-SP, and 832 for MCC-BM50-AC (see nomenclature defined below in 2.11).

A 5-s T_{1C} filter[72] was used to remove signals from segments with short ^{13}C spin-lattice relaxation times T_{1C} due to fast segmental motions, such as non-crystalline cellulose C6 side groups, retaining the sharp crystalline-C6 peaks of cellulose I and II, which are well resolved. The same numbers of scans as for the multiCP spectra were averaged. Direct polarization with 2-s recycle delay was used to select signals of mobile segments with fast T_{1C} relaxation, yielding the band of non-crystalline cellulose C6 complementary to the T_{1C}-filtered crystalline peaks. For all four samples 4096 scans were averaged. Zirconia rotors (Bruker Biospin) were used as received for magic-angle spinning of all samples.

2.10 Ethanolysis

Cellulose was converted using ethanolysis to test the reactivity of cellulose in the absence of solvent-promoted recrystallization. Briefly, 37% HCl was diluted to 0.1M in ethanol. Cellulose (0.25 grams) was mixed with 5 mL of 0.1M HCl-ethanol solution in a manner similar to the hydrolysis experiments and reacted at 130 °C for 1.5 hours. Ethanol vapor pressure limited

temperature selection as higher temperatures resulted in pressures that exceed the limits of the glass reactors used in this study. After the reaction, the mixture was centrifuged and the solid and liquid products were separated. The solid residue was additionally washed with ethanol, dried at 65 °C and weighed to determine conversion.

2.11 Sample Nomenclature

MCC is used as an abbreviation for microcrystalline cellulose throughout the text. For convenient reference, Table 1 provides suffixes that are used to denote various treatments of MCC.

Table 1. Suffixes used to denote treatment of microcrystalline cellulose (MCC).

Suffix to MCC	Sample Treatment
-BM50	Ball-milled for the indicated time duration
-BM50-HLW150	Ball-milled for the indicated time duration, then subjected to hot liquid water treatment at the indicated temperature
-BM50-AC	Ball-milled for the indicated time duration, then subjected to acid hydrolysis with 0.1 M HCl, for 1 hour, at 150 ℃
-BM50-SP	Ball-milled for the indicated time duration, then subjected to simulated sample treatment. The simulated sample treatment involved exposure of sample to 0.1 M HCl at room temperature for 10 minutes followed by 5 minute heating up to 150 ℃. After reaching temperature, sample was cooled rapidly and washed with acetone.

3. Results and Discussion

Reaction engineering models require qualitative knowledge of the relevant reaction pathways and quantitative knowledge of the relevant transport, thermodynamic, and especially kinetic parameters. Cellulose hydrolysis models typically have one or more parallel pathways describing hydrolysis of amorphous and crystalline cellulose, each with its own rate parameter.[41, 45, 73, 74] The rate constants used to describe hydrolysis of amorphous cellulose are typically greater

than those describing hydrolysis of crystalline cellulose, a decision which has been justified by rapid initial weight loss and decrease of degree of polymerization, followed by a leveling of reaction rate.[40, 41, 45, 75, 76] Such reasoning has been used to explain the observation of greater conversion rates of samples with lower crystallinity and motivates the use of decrystallizing pretreatments to increase cellulose reactivity.[28, 30, 39, 49] However, hydrolysis models that ascribe reactivity based on relative amounts of amorphous and crystalline cellulose do not take into account the fact that exposure to water promotes recrystallization of amorphous cellulose,[59, 60] meaning that even the qualitative features of the corresponding cellulose hydrolysis models may not be accurate. Models consisting of incorrect pathways can only aspire to data fitting, meaning that models that miss key pathways will lack predictive power. Development of predictive, structure-based models must account for all of the relevant underlying physical and chemical phenomena that affect reactivity. Accordingly, we began this study with a simple question: do current cellulose hydrolysis models contain all the pathways required for more than data fitting?

3.1 XRD Crystallinity and Reactivity

The first aim of this study was to reproduce the observations that cellulose decrystallization increases conversion and soluble product yields. The focus of this part of the study was measuring the reactivity of cellulose crystalline allomorph type I as it is the form that is present in lignocellulosic plant biomass.[77] Ball milling was selected as a mechanical method for decrystallizing cellulose.[24, 63] Accordingly, a family of cellulose samples with varying crystallinity was generated by subjecting Avicel microcrystalline cellulose (labeled MCC), a commonly studied cellulose I model substrate, to vibratory ball milling for varying amounts of time, from 10 to 50 min in 10 min increments ; Table 1 (section 2.11) provides sample naming conventions. Figure 1 provides representative X-ray diffractograms, obtained for MCC and the ball milled samples. As

expected, XRD indicates that ball milling progressively decreases MCC crystalline order. More specifically, the sharp peaks of MCC, assigned in the literature to diffraction from the 101, 10ī, 021, 200, and 040 crystalline planes,[47] broaden and decrease in intensity after ball milling.[78] The x-ray diffractogram of the most aggressively treated sample, MCC-BM50, is nearly featureless. Ball milling for durations greater than 50 min resulted in sample darkening which we took as evidence of formation of degradation products. Charring would have added unwanted complexity to the analysis and visual discoloration therefore placed an upper limit on the severity of the ball milling treatment.

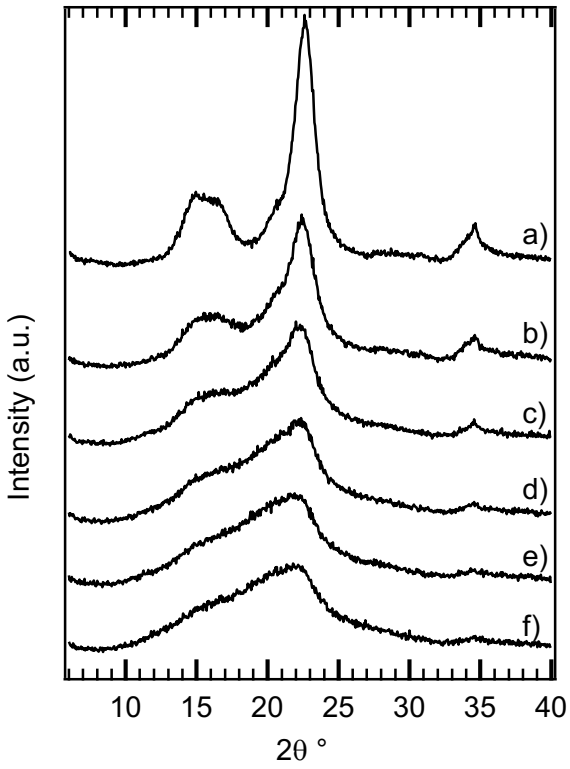

Figure 1. X-ray diffractograms of progressively ball-milled cellulose samples: a) Avicel-PH101, b) MCC-BM10, c) MCC-BM20, d) MCC-BM30, e) MCC-BM40, f) MCC-BM50.

Numerous methods have been proposed for quantifying cellulose crystallinity using characterization techniques such as XRD (peak height, amorphous subtraction, peak fitting,

Rietveld modelling), NMR (peak integration), Raman spectroscopy (peak heights), and Infrared spectroscopy.[47, 79-81] Estimated crystallinity values can be method dependent, pointing to issues of absolute quantification of non-crystalline cellulose.[47] To estimate crystallinity and correlate its trends to observed reactivity, we used Segal's method as a facile and most popular method, with the caveat that the method is best used as a qualitative indicator of crystallinity rather than a quantitative one.[47, 66] For precision, we term crystallinity measured using the Segal analysis method of XRD data, "Segal crystallinity". XRD data were used to calculate cellulose relative crystallinity and corresponding values are plotted in Figure 2 (black triangles). Segal crystallinity decreased with increasing ball milling time from 92% for MCC to 35% for MCC-BM50.

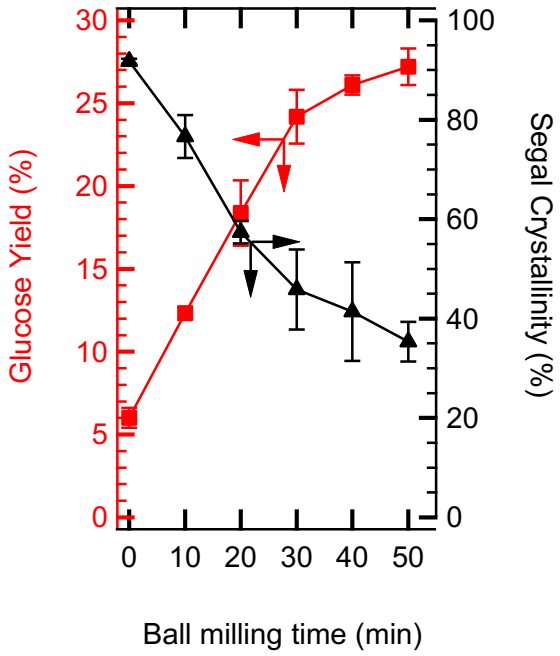

Figure 2. Glucose yield (■) and XRD Segal crystallinity (▲) of ball-milled cellulose samples plotted versus ball milling time.

To determine the effect of the mechanical treatment on reactivity, the ball-milled samples were subjected to acid hydrolysis at standard conditions (0.1 M HCl, 150 °C, 1 hour) and soluble product yields and conversion were measured. In all cases, glucose was the main product, with

trace amounts of HMF and cellobiose. Accordingly, measured glucose yields are plotted alongside the Segal crystallinity data in Figure 2 (red squares). As expected,[38] glucose yields increased with increased ball milling time, with the maximum obtained for MCC-BM50 (27±1 %). In all cases, mass balance between soluble products and recovered cellulose closed to within 8% (see Figure S1 in SI, red squares), consistent with losses during solids recovery and indicating that water-soluble glucose oligomers were minor byproducts; this was further supported by the fact that cellobiose yields were always less than 0.1% and measurable oligosaccharide yields were less than the estimated detection limit (0.005%). Accordingly, Figure 1 confirms that decreased Segal crystallinity and a commensurate increase of glucose yield are the apparent main effects associated with ball milling pretreatment, consistent with previous literature reports and establishing a baseline for more detailed experiments.[38, 43]

After the acid treatment, the residual solids were collected, washed with acetone, dried, and analyzed to determine the effect of the treatment on cellulose crystallinity. Acetone wash was employed to remove water from the sample and prevent changes in crystallinity during water drying, as reported previously.[82] In control tests, the XRD diffractogram did not change appreciably after treatment with acetone and subsequent drying, indicating that the method successfully avoided introduction of artifacts (see Figure S2).[61, 82, 83] Figure 3 provides the corresponding x-ray diffractograms of the acid hydrolyzed samples (see Table 1 for nomenclature). The characteristic profile of MCC is recovered after acid treatment, and the broad features of the ball-milled samples are no longer observable after treatment (compare to Figure 1). While the intensities of the main peaks are less than observed for the precursor MCC, the main diffraction peaks are clearly identifiable after acid treatment of even the most aggressively ball-milled sample, indicating that the acid hydrolysis treatment at least partially restores cellulose crystallinity.

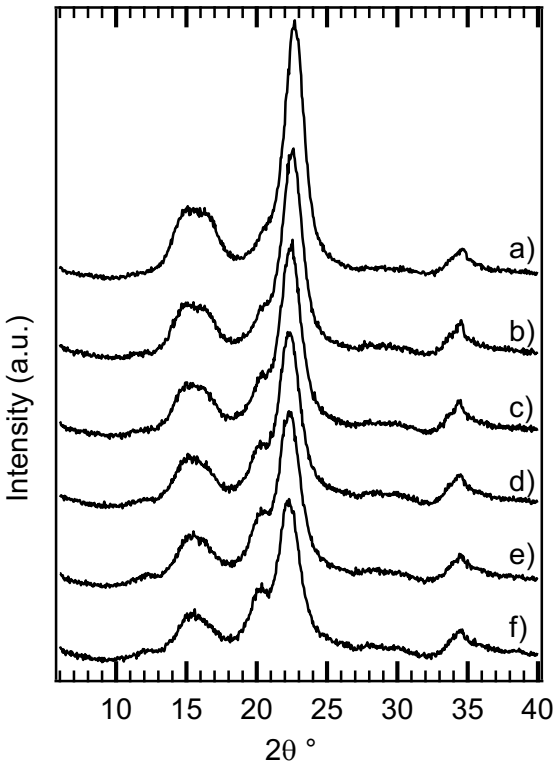

Figure 3. X-ray diffractograms of progressively ball-milled cellulose samples after 0.1 M HCl acid treatment at 150 °C for 1 hour: a) Avicel-PH101, b) MCC-BM10-AC, c) MCC-BM20-AC d) MCC-BM30-AC, e) MCC-BM40-AC, f) MCC-BM50-AC.

XRD Segal crystallinities of the acid treated samples were calculated as before and are plotted in Figure 4 as red squares. As expected from Figure 3, Segal crystallinity increases following acid hydrolysis compared to the ball-milled samples (black triangles); for example, the calculated Segal crystallinity of MCC-BM50, the most aggressively treated MCC sample, increases from 35% to nearly 86% after acid treatment. The magnitude of the Segal crystallinity increase depends on the ball milling time, with the greatest increase observed for the most aggressively ball-milled samples. The amorphous-crystalline cellulose reactivity theory would explain the observation of increased crystallinity as preferential hydrolysis of amorphous cellulose during acid treatment.[45] However, this explanation does not account for the spontaneous

recrystallization of cellulose that occurs during water exposure under non-hydrolytic conditions, a phenomenon reported several times but never connected directly with cellulose reactivity.[59, 60] Accordingly, we continued our study by attempting to isolate the effects of water-promoted recrystallization from hydrolytic effects.

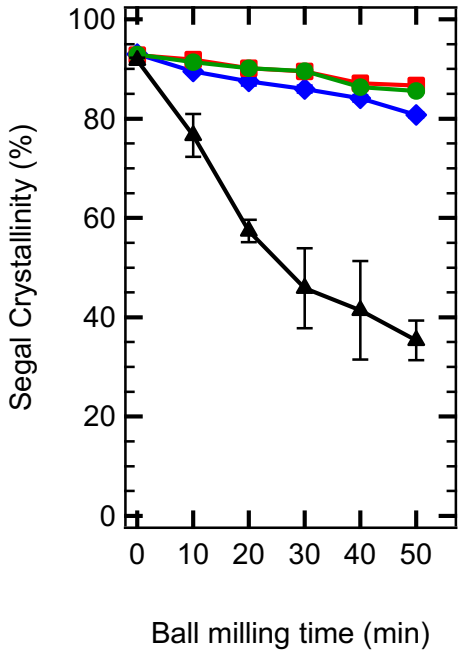

Figure 4. XRD Segal crystallinity of cellulose samples after ball milling (▲), acid hydrolysis (AC) (■), hot liquid water (HLW) (◆), and simulated sample preparation (SP) (●) treatments.

3.2 Water-Promoted Recrystallization

To isolate the effects of water-promoted recrystallization from hydrolysis of amorphous cellulose, we treated the MCC-BM samples by exposing them to hot liquid water (HLW, see Table 1) at the same temperature and reaction time as in the acid hydrolysis treatment, but without acid. Figure S3 shows the diffractograms of the HLW-treated samples. The qualitative XRD features obtained for the HLW are similar to those corresponding to samples subjected to acid hydrolysis, with the HLW treatment promoting recovery of the sharp diffraction peaks ascribed to crystalline cellulose. Figure 4 plots the Segal crystallinity values of samples that have undergone HLW

treatment (blue diamonds), showing that HLW treatment increases crystallinity to values similar to those observed after acid hydrolysis treatment. Unlike acid hydrolysis, HLW treatment resulted in soluble product yields of less than 0.5%. Mass balance closure was 103±2% (see Figure S1 blue diamonds), indicating that preferential conversion of amorphous regions to soluble products could not possibly account for the increased crystallinity. Instead, phase transition from amorphous to crystalline cellulose is implicated.

Comparing diffractograms obtained after hydrolytic and HLW treatments indicate that water-promoted cellulose recrystallization must occur in parallel with hydrolysis. The implication therefore is either that crystallinity plays at most a secondary role in reactivity or that cellulose hydrolysis models should be modified to include a cellulose recrystallization pathway that competes with hydrolysis. To differentiate between these two scenarios, the next step was to investigate the differences in the soluble product yields of decrystallized and recrystallized samples. MCC-BM50 was selected for studying the effects of recrystallization on product yields as the most highly decrystallized sample considered in this work that was therefore expected to elicit the greatest response to recrystallization treatment. Samples with varying degrees of recrystallization were generated by treating MCC-BM50 in HLW at 110, 130, and 150 °C (labeled as MCC-BM50-HLW110, 130, and 150 respectively). These samples were then subjected to acid hydrolysis at the same conditions as before (0.1 M HCl, 150 °C, 1 hour). Table 2 provides glucose yields and Segal crystallinity values obtained for the three HLW-treated samples. The same data are provided for MCC, MCC-BM50, and MCC-BM10 for comparison. After HLW treatment, the Segal crystallinities of MCC-BM50-HLW110, 130, and 150 are similar to one another and are significantly greater than that of MCC-BM50 prior to acid or water treatment. However, glucose yields obtained from acid hydrolysis of the HLW samples are the same to within uncertainty as

those obtained for MCC-BM50. Reaction models that explain reactivity using different rate constants for amorphous and crystalline cellulose would predict that the yields obtained from hydrolysis of the HLW samples should be similar to those obtained for MCC-BM10, which is not observed and is a clear breakdown of existing cellulose hydrolysis models.

Table 2. XRD Segal crystallinities and glucose yields obtained from hydrolysis of MCC subjected to different treatments. Reaction conditions: 0.1M HCl, 150 °C, 1 hour.

Sample	Segal Crystallinity (%)	Glucose Yield (%)
MCC	92	6 ± 1
MCC-BM10	77 ± 4	12 ± 0.4
MCC-BM50	35 ± 4	27 ± 1
MCC-BM50-HLW110	77 ± 1	28 ± 2
MCC-BM50-HLW130	79 ± 1	26 ± 2
MCC-BM50-HLW150	81 ± 1	24 ± 3

The data in Figure 4 and Table 2 suggest that the crystallinity of ball-milled cellulose prior to contact with water may not be the most appropriate measurement for understanding reactivity. In particular, the rate of water-promoted recrystallization of amorphous cellulose is not clear and simply contacting water may be sufficient to recrystallize amorphous cellulose.[59] The effects of water-promoted recrystallization thereby make cellulose crystallinity a moving target, even before the potential effects of hydrolysis on crystallinity are considered. To estimate cellulose crystallinity at the onset of hydrolysis, MCC-BM samples were subjected to a treatment identical to that used to generate glucose yield data, including a 10-min mixing period and a 5-min heating period. However, instead of permitting the reaction mixture to remain at temperature for 1 h, the reaction

mixture was rapidly quenched in an ice bath, filtered, and the solid rinsed with acetone to prevent further exposure to the aqueous solution. Samples treated in such a manner were labeled with an additional -SP descriptor to denote the sample preparation treatment and analyzed for the effects of the simulated sample treatment on crystallinity (See Table 1).

The x-ray diffractograms obtained for SP samples (provided as Figure S4 in the SI) are qualitatively similar to those obtained from the HLW and AC samples, indicative of crystallinity recovery after the simulated sample treatment. Figure 4 plots the values of Segal crystallinity of the samples subjected to simulated sample preparation treatment (green circles), showing that the estimated crystallinities of the SP samples agree within error with those of the HLW and AC samples. As before, mass balance considerations do not support the theory of preferential solubilization of amorphous cellulose during sample preparation (both cellulose conversion and yields of soluble products were <1%). Therefore, results from the simulated sample treatment indicate that water promoted cellulose recrystallization is nearly complete during sample preparation and heat up. In comparison, any changes in crystallinity due to conversion of amorphous cellulose to soluble products within that timeframe occur more slowly – if at all. These results provide an explanation for the similar glucose yields of MCC-BM50 and MCC-BM50-HLW samples presented in Table 2. By the time release of soluble products has begun, MCC-BM50 has reached the same level of crystallinity as MCC-BM50-HLW150, suggesting that the samples are structurally identical during hydrolysis, hence, the equivalence of their reactivity. Moreover, Figure 4 suggests that crystallinity of the dry sample fed to the reactor is not even especially relevant to the state of the sample being converted to soluble products and instead that the more meaningful correlation might be between reactivity and the crystallinity measured after the simulated sample preparation treatment as it is the state that undergoes hydrolysis.

Figure 5 re-plots the glucose yields versus their corresponding values of Segal crystallinity measured for ball-milled (black triangles) and SP samples (green circles). As expected based on the literature in this field[38, 40] and as anticipated from Figure 2, glucose yields increase with decreasing substrate Segal crystallinity, provided that crystallinity is measured for the dry sample prior to contacting water. In contrast, when glucose yields are plotted with values of crystallinity measured after simulated sample preparation treatment instead of a linear relationship with finite slope, the glucose yields are nearly invariant with crystallinity. While glucose yields increase, the Segal crystallinity does not, indicating a lack of predictive correlation, when crystallinity is measured correctly at the onset of hydrolysis. As a result, including parallel pathways for hydrolysis of amorphous and crystalline domains in hydrolysis reaction models may be a numerical approach to capture observed glucose yield data, but parallel pathways are not physically meaningful since no correlation exists between crystallinity at the onset of hydrolysis and glucose yields.

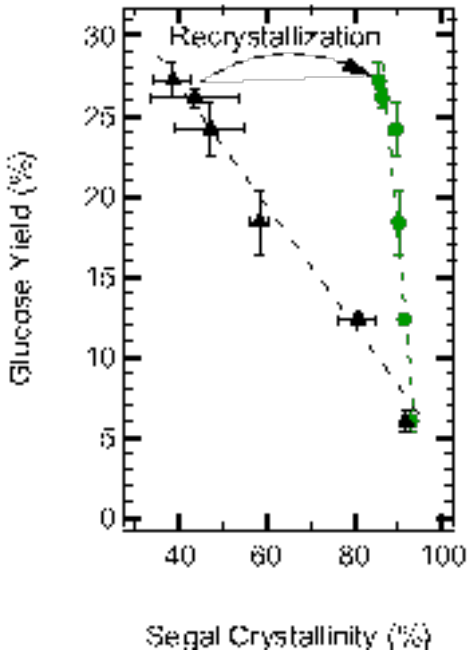

Figure 5. Glucose yield plotted as a function of XRD Segal crystallinity measured after ball milling (▲) and after sample preparation and heat up (●). The arrow indicates the effect of recrystallization on the reactivity-crystallinity correlation.

Figure 5 suggests a complete re-interpretation of cellulose hydrolysis models; however, the validity and strength of that conclusion may be limited by the method selected for analyzing cellulose structure and estimating crystallinity, as the Segal method has shortcomings for quantitative measurements of crystallinity. Moreover, mechanical decrystallization clearly results in structural changes that increase cellulose reactivity, while water-promoted recrystallization restores apparent Segal crystallinity but with negligible effects on reactivity. This leads to two simple questions: 1) can Segal crystallinity measurements be trusted on their own for model development? and 2) what occurs during decrystallization-recrystallization that affects XRD diffractograms reversibly, but not reactivity?

3.3 Raman and ssNMR Analysis

To answer these questions, we expanded the analysis of the various cellulose samples to include additional instrumentation. As a starting point, we initially selected the Segal method for quantifying crystallinity, as this is the most widely used cellulose characterization technique.[47] However, cellulose is a complex polymer with several different allomorphs, and many different techniques have been developed for probing cellulose structure, and especially estimating its crystallinity.[47] Based on this rationale, Raman spectroscopy and solid-state nuclear magnetic resonance (ssNMR) were selected as well-documented cellulose crystallinity estimation techniques that probe qualitatively different aspects of cellulose structure than does XRD.[47, 80] Whereas XRD is sensitive to the periodic arrangement of atoms in the cellulose lattice, Raman is sensitive to chain vibrations attributable to skeletal configuration[84] and NMR can detect differences in atomic environment associated with polymer conformation and packing.[85] The distinct physical basis of the three methods means that making qualitatively (and quantitatively) similar observations with all three can answer the question about the reliability of different methods of crystallinity estimations for model development. Considering that Raman and especially NMR provide additional information not captured by XRD, the additional techniques also have potential for answering the question about the different reversible and irreversible changes that cellulose undergoes during ball milling.

Figure 6 plots the Raman spectra of MCC and MCC-BM50 after various treatments and specific peaks at 380 and 1096 cm^{-1} associated with crystallinity are highlighted. Raman spectra of the entire series of samples are presented in Figures S5 to S8. The Raman spectrum of MCC-BM50 exhibits a general loss of intensity and blurring of fine spectral features compared with MCC; both of these changes are attributable to a loss of crystallinity.[80] Spectra b, c and d, in Figure 6 show that exposure to aqueous conditions, including acid hydrolysis (MCC-BM50-AC), hot

liquid water (MCC-BM50-HLW150), or simulated sample preparation (MCC-BM50-SP) all result in increased intensity of the bands characteristic of crystallinity, specifically those appearing at 380 and 1096 cm^{-1}.[80] In fact, the Raman spectra of the various water-treated samples are nearly indistinguishable from one another, though recrystallization does not recover the intensities of the crystalline peaks to the levels of the precursor MCC sample. Accordingly, Raman analysis shows the same qualitative behavior as does XRD, lending credibility to the Segal interpretation of the XRD data.

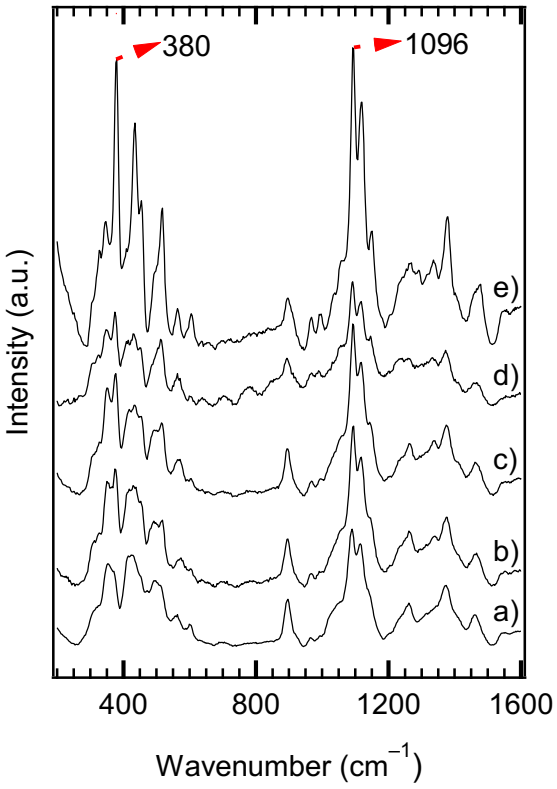

Figure 6. Raman spectra of selected cellulose samples: a) MCC-BM50, b) MCC-BM50-HLW, c) MCC-BM50-SP, d) MCC-BM50-AC, and e) Avicel MCC. Peaks associated with crystallinity at 380 cm─1 and 1096 cm─1 are indicated with red arrows.

To gain greater insight, selected samples were further analyzed using quantitative ^{13}C ssNMR. Specific focus was placed on the C4 and C6 regions of the NMR spectrum, as these

regions contain distinguishable contributions from carbons in crystalline interior chains and non-crystalline surface or truly amorphous chains.[85] In fact, heretofore, we have adopted typical convention and not differentiated between non-crystalline and amorphous cellulose, as XRD and Raman are cannot distinguish them from each other. The most severely decrystallized sample, MCC-BM50, and its recrystallized analogs were studied and compared to the untreated MCC. Their C4 and C6 signals are plotted in Figure 7, showing that ball milling results in almost complete elimination of the crystalline cellulose I signals between 87 and 92 ppm and 64 and 68 ppm. The bands between 80 and 87 ppm and 58 and 64 ppm are broader than those of the non-crystalline surface chains in untreated MCC and can therefore be assigned to truly amorphous cellulose; surface chains are indeed not to be expected since almost no crystals exist. Non-hydrolytic or hydrolytic treatment using any of the previously described methods increases the relative intensity of the C4 signal of the crystalline chains (see spectra of MCC-BM50-SP and MCC-BM50-AC), again consistent with water-promoted recrystallization. After recrystallization the band between 80 and 87 ppm was displaced to a lower field chemical shift and recovers the narrower features of the non-crystalline surface chains, rather than amorphous cellulose. As with XRD and Raman, NMR indicates that most of the recovery of the crystalline signal is observed after contact with water and heat up with only minor additional increase after prolonged acid hydrolysis.

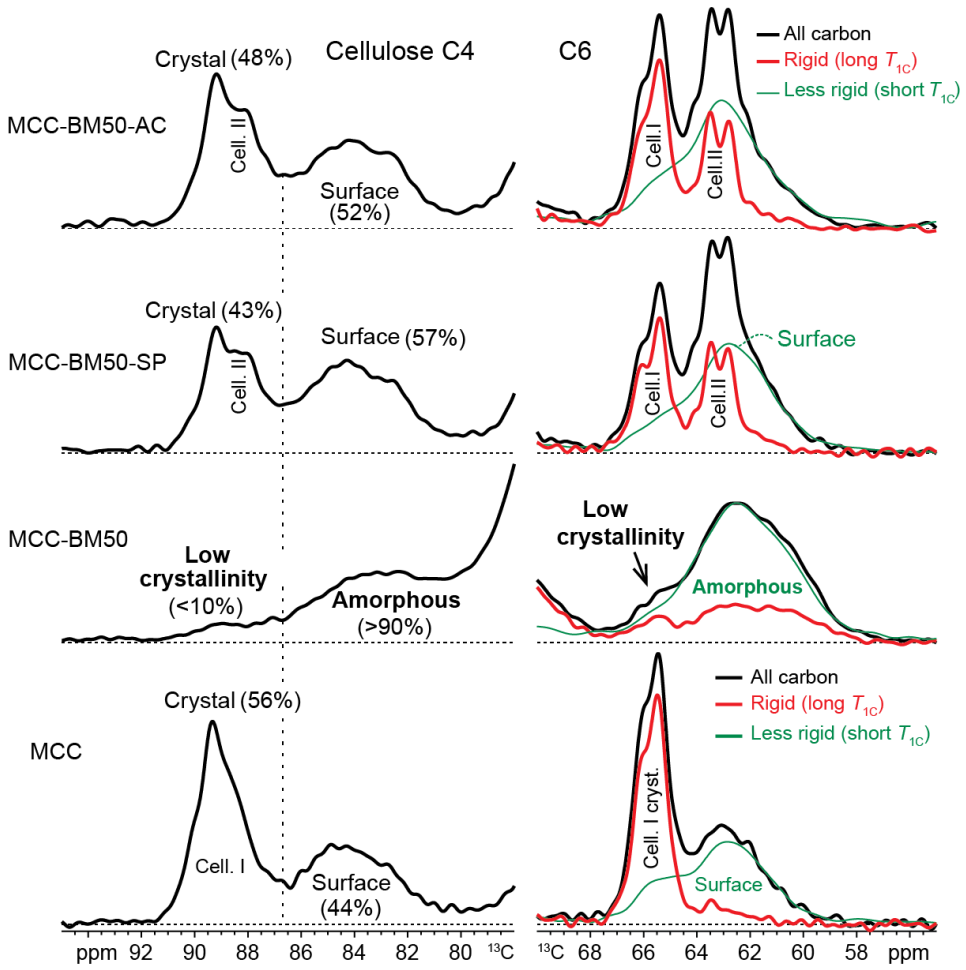

Figure 7. The C4 and C6 ^{13}C NMR spectra of selected cellulose samples. The black curve represents the overall spectra; the red curve is signal from domains with long T_{1C} relaxation times, and the green curve is signal from regions with short T_{1C} relaxation times.

Comparing the C6 regions of MCC and MCC-BM50 shown in Figure 7 (right column) confirms that ball milling decrystallization decreases the signal of interior crystalline regions and increases the amorphous content. All previous arguments led us to expect that recrystallization would result in recovery of spectral intensity and peak shape in the C6 carbons analogously to those observed for C4 carbons. However, while the interior crystalline signal partially recovered its initial shape an intensity, the intensity between 60 and 64 ppm also increased. Moreover, the shape of the features in the C6 surface region changed from a single broad band to include a

narrower doublet. The new feature can be attributed to crystalline cellulose II,[85] a distinct allomorph of cellulose not present in lignocellulosic plant biomass.[77] This assignment is confirmed by spectral editing in Figure 7, which resolves the cellulose II doublet when the band of the more mobile non-crystalline chains is suppressed based on their faster spin–lattice relaxation. Although formation of cellulose II after ball milling is not specifically considered in common cellulose hydrolysis models,[74] recrystallization of amorphous cellulose as both cellulose I and II has been reported in the previously in the literature.[56, 86] Our study now shows that recrystallization of cellulose I and II must have reactivity implications.

Coexistence of cellulose I and cellulose II is crucially important for reactivity and the reaction mechanism since cellulose II is often the more reactive allomorph.[87] In the NMR spectra cellulose II interior signal coincides with surface signal from cellulose I. By separating cellulose C6 signals with long (crystalline) and short (non-crystalline) T_{1C} relaxation times, see Figure 7, we deconvolved the spectra and quantified the cellulose I, II, and non-crystalline surface content. The results, presented in Table 3, show that after one hour of hydrolysis (MCC-BM50-AC) the cellulose I content is increased by 3% relative to simulated sample treatment (MCC-BM50-SP), the non-crystalline decreases by about the same amount, while cellulose II appears to remain the same. However, the observed changes cannot account for the glucose yield (28%), which indicates that both cellulose I and II fractions are being hydrolyzed to glucose. Both C6 deconvolution and the C4 region shows that the recrystallized cellulose has ~4-5% greater non-crystalline surface content when compared to the starting MCC. Since overlap between interior and surface chain signals from either allomorph in the C4 region is minor, estimation of the surface content based on C4 region could be more reliable. This could imply that in addition to the more reactive cellulose II, the composite cellulose sample could have greater accessible surface area available

for hydrolysis. Greater relative surface chain content could potentially mean smaller crystallite size, and cellulose with smaller crystallite size has been reported to exhibit greater swelling and solubility,[88] suggesting possible correlation with reactivity towards acid hydrolysis.

Table 3. Cellulose I, cellulose II, and non-crystalline content calculated by deconvolution of the C6 signal in the NMR spectra.

Sample	Cellulose I (%)	Cellulose II (%)	Non-crystalline (%)
MCC	47±1	0	53±1
MCC-BM50	3.5±1	0	96.5±1
MCC-BM50-SP	25±2	18±2	57±3
MCC-BM50-AC	28±2	17.5±2	54.5±3

Given the surface chain content and the presence of cellulose II in recrystallized cellulose, we revisited the XRD and Raman spectra for additional insight that might have been missed on first analysis. In fact, a distinguishable peak at 12.2° (see Figure S9) was attributed to the $1\bar{1}0$ crystalline planes of cellulose II. The FWHM of the main peak at 22.5° increases with increasing ball milling time (shown in Figure S10), further indicating decreasing crystallite size. Literature XRD analysis of cellulose I and II mixtures has been carried out by mixing pure allomorphs and varying their content.[89]

We explored using Figure S9 for quantification. Cellulose II exhibits characteristic XRD features that distinguish it from cellulose I[90] which can allow deconvolution of the diffractograms to estimate the content of each allomorph and correlate it to the reactivity of a sample.[89] In addition, the crystallite size can be estimated from the full width at half maximum (FWHM) of corresponding diffraction peaks, which provides further structural information that can be

accounted for in developing a hydrolysis model.[89] This approach, however, is not applicable here since crystallite size likely varies with decrystallization and potentially recrystallization.[44] Furthermore, the interlayer distance has been shown to vary with crystallite size,[88] thus affecting the position of the Bragg's diffraction angle. Quantitative data of cellulose I and II from NMR analysis could be used to decrease the number of variables, but the positions of the underlying cellulose I and II peaks remains unknown. Unfortunately, due to the many degrees of freedom of fitting the XRD diffractograms an unambiguous deconvolution by fitting diffraction peaks of the cellulose I and cellulose II and calculating their crystallite size cannot be achieved, preventing correlation of crystallite size to reactivity. In the end, XRD diffractograms allow us to conclude that decrystallization-recrystallization leads to formation of a complex mixture of cellulose I and II, potentially with reduced crystallite size compared with the starting material – all of which are qualitatively in agreement with ssNMR.

3.4 Conversion of Cellulose in Non-Recrystallizing Solvent

Having answered the question about XRD reliability, the next question then becomes: Are the cellulose I/II and potentially size-reduced crystallites simply a more specific description of the reactive form of cellulose that accounts for the effects of mechanical decrystallization on hydrolysis reactivity? Or, is the reactivity of truly amorphous cellulose different from that of either the starting material or the cellulose I/cellulose II mixture? Hydrolysis treatment cannot answer this question since exposure to water collapses amorphous cellulose into the cellulose I/cellulose II mixture. Instead, ethanolysis is a suitable model reaction for studying the reactivity of amorphous cellulose compared with that of the recrystallized mixture. The mechanism of ethanolysis is similar to hydrolysis[91] and yet previous work indicates that organic solvents do not promote rapid recrystallization of amorphous cellulose under non-hydrolytic conditions.[60] Figure

S11 provides the XRD diffractogram of MCC-BM50 treated in ethanol at elevated temperature (130 °C, 1.5 h). The XRD diffractogram sharpens slightly after the treatment, although not to the extent that occurs in water, indicating that solvent-promoted recrystallization is suppressed when using ethanol.

Comparing ethanolysis rates for MCC, ball-milled MCC, and ball-milled and recrystallized MCC can provide relative reactivity information for crystalline cellulose I, amorphous cellulose, and the recrystallized cellulose I/cellulose II mixture, respectively. Accordingly, the ethanolysis conversions of MCC (as a baseline), MCC-BM50 (decrystallized), and MCC-BM50-HLW150 (recrystallized) were measured at standardized conditions (0.1M HCl in ethanol, 130 °C, 1.5 h). The primary products of ethanolysis, ethyl glucopyranoside, ethoxymethyl furfural and ethyl levulinate, are ethanol soluble[91] so that conversion measurements alone provide unambiguous indications of reactivity. Accordingly, Table 4 provides the ethanolysis conversion data, showing that MCC, MCC-BM50, and MCC-BM50-HLW indeed exhibit differences in reactivity under conditions where solvent-promoted recrystallization does not occur. Specifically, the amorphous cellulose content of MCC-BM50 is more reactive than the recrystallized substrate, resulting in 41% conversion of the decrystallized sample compared with 13% under the same conditions for the recrystallized one. In comparison, cellulose I (MCC) is nearly unreactive. The data in Table 4 therefore establish that the cellulose I/cellulose II mixture is much less reactive than amorphous cellulose, i.e., cellulose I/cellulose II is not simply a more specific description of the reactivity of ball milled cellulose, but actually distinct.

Table 4. Conversion, change in XRD Segal crystallinity values, and apparent kinetic rate constant of selected cellulose samples subjected to ethanolysis treatment. Studied samples were MCC, ball-milled cellulose MCC-BM50, and ball-milled and hot liquid water recrystallized MCC-BM50-HLW.

Sample	Conversion (%)	Initial crystallinity (%)	Final crystallinity (%)	Crystallinity change (%)	Ethanolysis k (h^{-1})
MCC (baseline)	2 ± 1	92	93	1	0.016 ± 0.009
MCC-BM50 (decrystallized)	41 ± 2	35	81	46 ± 1	0.35 ± 0.024
MCC-BM50-HLW150 (recrystallized)	13 ± 1	81	84	3 ± 1	0.09 ± 0.012

To investigate ethanolyzed cellulose further, the treated samples were analyzed using XRD. The corresponding diffractograms are presented in Figure S12, and estimated changes in crystallinities are provided in Table 2. Cellulose I Segal crystallinity is not affected by ethanolysis, as MCC crystallinity remains unchanged at 93% after treatment. In contrast, the Segal crystallinity of MCC-BM50 increases sharply from 35 to 81% after ethanolysis. The low solvent recrystallization potential of ethanol as shown in Figure S11, suggest that the increase in Segal crystallinity of MCC-BM50 after ethanolysis could be attributed partly to preferential conversion of amorphous cellulose to soluble products. A potential parallel mechanism for increasing crystallinity could be scission of reactive bonds and relaxation of chains into crystalline organization.[92] In contrast, the rapid increase of cellulose crystallinity during hydrolysis is primarily due to solvent-induced recrystallization and not conversion of amorphous cellulose to soluble products as revealed by Figure S1 and Figure 4. Remarkably, the results and interpretation are similar to the original model suggested by Philipp et al.,[45] i.e. differential rates of conversion

of amorphous and crystalline cellulose, except we find that this occurs only under ethanolysis and not hydrolysis conditions. Finally, the x-ray diffractogram and Segal crystallinity of MCC-BM50-HLW150 do not change after ethanolysis, again consistent with water-promoted recrystallization reaching effective completion after water exposure even before the onset of hydrolysis.

3.5 Updating the Cellulose Hydrolysis Model

Table 3 establishes that the reaction mechanism describing hydrolysis of amorphized cellulose must include a recrystallization step for formation of the cellulose I/cellulose II mixture. However, what is less clear for reaction models is if a single rate constant can be used to describe the reactivity of the cellulose I/cellulose II mixture, irrespective of the degree of amorphization the sample had undergone prior to water-induced recrystallization. Put another way, is the cellulose I/cellulose II mixture functionally a single material or does it encompass a range of materials, each with different reactivities? In particular, previous work on cellulose reactivity implicates a potential role of degree of polymerization (DP).[REF] Previous studies[REF] indicate that ball milling cellulose leads to a reduction of DP, with DP decreasing monotonically with increasing ball mill intensity and duration.[REF] Therefore, the result of the decrystallization-recrystallization process might result in a family of materials with different DP characteristics and hence reactivities that differ based on the duration of the initial ball milling treatment that cannot be captured simply as a mixture of cellulose I and cellulose II.[REF]

To investigate further, hydrolysis yield data were converted into rate constants assuming a first order hydrolysis rate law, as is typically reported in the literature.[93] Further, we assumed that the hydrolysis data obtained from treatment of MCC were representative of highly recalcitrant crystalline cellulose and calculated its rate constant. Based on this assumption we then normalized Segal crystallinity values to estimate the amount of the two cellulosic species assuming that the

amorphous content completely converts to active recrystallized cellulose at the time of onset for hydrolysis, as XRD, Raman, and NMR indicate that MCC-BM50 consists almost completely of amorphous cellulose. Avicel MCC was assumed as a 100% crystalline cellulose with low reactivity and the samples ball-milled for intermediate durations were normalized to be a mixture of Avicel MCC and MCC-BM50 based on their Segal crystallinity.

Following this analysis method, the rate constant for hydrolysis of active recrystallized cellulose mixture could be determined by difference for all of the ball-milled samples, as shown in Figure 8. Interestingly, the data indicate that the rate constant is at most a weak function of the amount of active cellulose initially present, suggesting that – to within the limits of uncertainty – a single rate constant is appropriate for describing the reactivity of the recrystallized cellulose I/cellulose II mixture. Using the NMR data of cellulose I and II content and the glucose yields, we calculated the hydrolysis rate constants as 0.22 h^{-1} for cellulose I and 0.48 h^{-1} for cellulose II. Further we

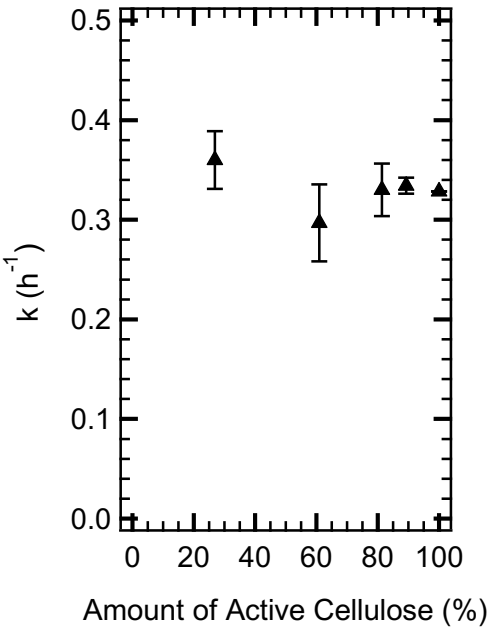

Figure 8. Kinetic rate constant of hydrolysis of active recrystallized cellulose plotted versus its amount calculated from XRD Segal crystallinities of ball-milled cellulose.

calculated a composite rate constant by weight averaging the contribution of each allomorph, arriving at 0.36 h^{-1} for active cellulose, which is consistent with the values presented in Figure 8, supporting the above interpretation.

While the current data are sufficiently explained using a single rate constant for active cellulose hydrolysis, the values of this rate constant may depend on additional sample-dependent factors, such as degree of polymerization. In particular, the active cellulose formed here must have DP equal to or less than that of the parent material since formation of new glycosidic bonds during any of the thermal or acidic treatments used here is not expected. Therefore, the reactivity of active cellulose found here may in part be a reflection of DP effects, as well as coexistence of cellulose I and cellulose II. Careful study of the effect of DP on cellulose I and cellulose II reactivity is recommended to clarify this issue. The work presented here should be considered during development of the DP study, since just as crystallinity changes under non-solubilizing conditions, so too might DP.[REF] Lastly, cellulose reactivity depends on source, which is another factor to be considered.[REF]

Structural characterization and reactivity data presented here suggest revision of the classical hydrolysis mechanism of decrystallized cellulose. Specifically, addition of two new pathways – recrystallization of amorphous cellulose and hydrolysis of recrystallized cellulose to glucose – should be included in the overall reaction network. Figure 9 summarizes the new model. Exposure of amorphous cellulose to aqueous conditions leads to water-promoted recrystallization as a new form of cellulose, which is a combination of cellulose I and cellulose II with greater surface content and/or decreased crystallite size compared with the original. Since its structural characteristics are not yet entirely clear, Figure 9 retains the label of the recrystallized material as “active cellulose”, echoing previous terminology used in the pyrolysis literature.[94] Hydrolysis occurs via parallel

pathways involving crystalline cellulose I, active cellulose, and any trace amorphous cellulose remaining in the sample during and after water-induced recrystallization.

The rates of all reactions shown in Figure 9 can be described by their own rate constants. The current study did not aim to quantify these rates; however, the data presented here allow identification of the relative order of their magnitudes. Specifically, the experimental data make clear that the rate constant for recrystallization of amorphous cellulose to active cellulose (k_2) is much greater than the rate constant for active cellulose hydrolysis (k_4). The rate constant for hydrolysis of crystalline cellulose I (k_1) is less than either k_2 or k_4. If recrystallization could somehow be prevented, ethanolysis data suggest that hydrolysis rate constant of amorphous cellulose, k_3, would be greater than all other hydrolysis rate constants. Future studies can be performed to measure these rate constants, with these general trends as guidance. As mentioned previously, the effect of DP on hydrolysis rate constants should be included in these studies.

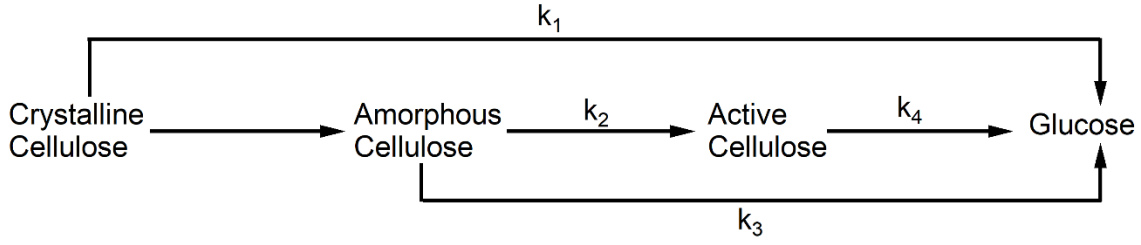

Figure 9. Proposed updated cellulose hydrolysis model that involves a conversion of crystalline to amorphous decrystallization pathway. Water-promoted recrystallization is incorporated by a transformation of amorphous cellulose to active crystalline cellulose. The three types of cellulose exhibit different reactivity described by a respective rate constant.

The updated hydrolysis model presented here implies that studies interpreting the reactivity of decrystallized cellulose in aqueous conditions as hydrolysis of amorphous cellulose are likely observing hydrolysis of what we have termed active cellulose. Since mechanical amorphization is

a common method of increasing cellulose reactivity, the results of this study can be generalized.[28, 38] Recrystallization of amorphous cellulose in liquid water has been reported to occur even at room temperature.[59-61] Similarly, we observed sharpening of the XRD peaks of cellulose wetted for 1 hour at room temperature (data not shown), although not to the same extent as the hot liquid water treated samples. This indicates that water-induced recrystallization is an activated process; presence of acid could increase the rate of recrystallization by a scission-relaxation mechanism.[92] This rapid transformation suggests that depolymerization of truly amorphous cellulose cannot be realized in aqueous conditions even in the mild conditions of enzymatic hydrolysis. This indicates that the benefits of decrystallization are diminished when water is used as the reaction medium. Consequently, the recrystallizing effect of water renders mechanical decrystallization less effective than it has the potential to be. Therefore, an alternative approach for cellulose deconstruction is depolymerization of decrystallized cellulose in solvents that do not promote recrystallization. In fact, this may account partially for the success of co-solvent based biomass deconstruction approaches.[95] Regardless of how it is achieved, circumventing water-promoted recrystallization can permit direct conversion of the highly reactive amorphous cellulose, with potential benefits such as use of more moderate reaction conditions, increased yields and selectivities of soluble products, and decreased processing costs.

4. Conclusions

The most common reaction model describing cellulose hydrolysis proposes that reaction occurs via parallel pathways involving amorphous and crystalline cellulose. Invariably in these models, the hydrolysis rate of amorphous cellulose is much greater than that of crystalline cellulose. While this reaction model appears to match the available data, experiments to date have not confirmed the reaction network that it implies. To examine the effects of decrystallization on

the cellulose hydrolysis reaction network, we investigated mechanical decrystallization and water-promoted recrystallization on cellulose reactivity. Ball milling cellulose decreases crystallinity and increases its hydrolysis reactivity, both of which appear to support the theory of highly reactive amorphous and recalcitrant crystalline regions. However, by exposing decrystallized cellulose to the aqueous environment of acid hydrolysis we discovered that rapid recrystallization occurs and that the phase transition is complete before the onset of hydrolytic solubilizaiton. These results contradict the current hydrolysis models describing cellulose hydrolysis as parallel reactions of amorphous and crystalline regions.

Ball-milled and recrystallized cellulose can be structurally distinguished from crystalline cellulose I precursor as a mixture of cellulose I and II using ssNMR. Decrystallization and recrystallization may also decrease crystallite size, confounding quantification of the various cellulose forms. Reacting decrystallized cellulose under ethanolysis conditions where solvent-promoted recrystallization is suppressed confirms that the reactivity of amorphous cellulose is greater than that of the recrystallized form. Consequently, we modified the current cellulose hydrolysis models by incorporating a pathway for recrystallization of amorphous cellulose to active crystalline cellulose. The reactivities of crystalline of cellulose I, amorphous cellulose, and active cellulose can be described using distinct reaction rate constants. Furthermore, the rate of recrystallization is greater than any of the hydrolysis rates. The knowledge provided here can serve for further development of structure-activity relationships and cellulose conversion models and for design of processes that avoid cellulose recrystallization.

Conflicts of interest.

The authors declare no conflicts.

Acknowledgments.

The U.S. National Science Foundation, Award No. 1554283, funded this work. The ssNMR spectrometer used was purchased with funds from Award No. 1726346. Sergio Granados-Focil (Clark University) provided helpful suggestions to the technical content of this study.

References

1. M. H. Langholtz, B. J. Stokes and L. M. Eaton, *2016 Billion-ton report: Advancing domestic resources for a thriving bioeconomy, Volume 1: Economic availability of feedstock*, 2016.
2. F. H. Isikgor and C. R. Becer, *Polymer Chemistry*, 2015, **6**, 4497-4559.
3. M. J. Climent, A. Corma and S. Iborra, *Green Chemistry*, 2014, **16**.
4. J. George and S. N. Sabapathi, *Nanotechnol Sci Appl*, 2015, **8**, 45-54.
5. H. Kargarzadeh, M. Mariano, D. Gopakumar, I. Ahmad, S. Thomas, A. Dufresne, J. Huang and N. Lin, *Cellulose*, 2018, **25**, 2151-2189.
6. H. Kang, R. Liu and Y. Huang, *Polymer*, 2015, **70**, A1-A16.
7. D. M. Alonso, J. Q. Bond and J. A. Dumesic, *Green Chemistry*, 2010, **12**.
8. R. Rinaldi and F. Schuth, *ChemSusChem*, 2009, **2**, 1096-1107.
9. L. R. Lynd, X. Liang, M. J. Biddy, A. Allee, H. Cai, T. Foust, M. E. Himmel, M. S. Laser, M. Wang and C. E. Wyman, *Curr Opin Biotechnol*, 2017, **45**, 202-211.
10. T. Endo, E. M. Aung, S. Fujii, S. Hosomi, M. Kimizu, K. Ninomiya and K. Takahashi, *Carbohydr Polym*, 2017, **176**, 365-373.
11. K. Wu, G. Feng, Y. Liu, C. Liu, X. Zhang, S. Liu, B. Liang and H. Lu, *Bioresour Technol*, 2018, **261**, 28-35.
12. B. Mostofian, C. M. Cai, M. D. Smith, L. Petridis, X. Cheng, C. E. Wyman and J. C. Smith, *J Am Chem Soc*, 2016, **138**, 10869-10878.

13. M. Mohan, R. Timung, N. N. Deshavath, T. Banerjee, V. V. Goud and V. V. Dasu, *RSC Advances*, 2015, **5**, 103265-103275.

14. J. A. Geboers, S. Van de Vyver, R. Ooms, B. Op de Beeck, P. A. Jacobs and B. F. Sels, *Catalysis Science & Technology*, 2011, **1**.

15. S. Sun, S. Sun, X. Cao and R. Sun, *Bioresour Technol*, 2016, **199**, 49-58.

16. R. W. Torget, J. S. Kim and Y. Y. Lee, *Industrial & Engineering Chemistry Research*, 2000, **39**, 2817-2825.

17. S. Deguchi, K. Tsujii and K. Horikoshi, *Green Chem.*, 2008, **10**, 191-196.

18. S. P. Chundawat, G. Bellesia, N. Uppugundla, L. da Costa Sousa, D. Gao, A. M. Cheh, U. P. Agarwal, C. M. Bianchetti, G. N. Phillips, Jr., P. Langan, V. Balan, S. Gnanakaran and B. E. Dale, *J Am Chem Soc*, 2011, **133**, 11163-11174.

19. D. Klemm, B. Heublein, H. P. Fink and A. Bohn, *Angew Chem Int Ed Engl*, 2005, **44**, 3358-3393.

20. G. SriBala, R. Chennuru, S. Mahapatra and R. Vinu, *Cellulose*, 2016, **23**, 1725-1740.

21. E. Johnson, *Biofuels, Bioproducts and Biorefining*, 2016, **10**, 164-174.

22. N. Sweygers, N. Alewaters, R. Dewil and L. Appels, *Sci Rep*, 2018, **8**, 7719.

23. L. R. Lynd, *Nat Biotechnol*, 2017, **35**, 912-915.

24. A. Bychkov, E. Podgorbunskikh, E. Bychkova and O. Lomovsky, *Biotechnol Bioeng*, 2019, **116**, 1231-1244.

25. S. P. Chundawat, G. T. Beckham, M. E. Himmel and B. E. Dale, *Annu Rev Chem Biomol Eng*, 2011, **2**, 121-145.

26. M. A. Rostagno, J. M. Prado, A. Mudhoo, D. T. Santos, T. Forster-Carneiro and M. A. Meireles, *Crit Rev Biotechnol*, 2015, **35**, 302-312.

27. B. Yang, Z. Dai, S.-Y. Ding and C. E. Wyman, *Biofuels*, 2014, **2**, 421-449.

28. M. Hall, P. Bansal, J. H. Lee, M. J. Realff and A. S. Bommarius, *FEBS J*, 2010, **277**, 1571-1582.

29. X. Zhao, L. Zhang and D. Liu, *Biofuels, Bioproducts and Biorefining*, 2012, **6**, 465-482.

30. L. T. Fan, Y.-H. Lee and D. R. Beardmore, *Biotechnology and Bioengineering*, 1981, **23**, 419-424.

31. Y. Pu, F. Hu, F. Huang, B. H. Davison and A. J. Ragauskas, *Biotechnol Biofuels*, 2013, **6**, 15.

32. R. Kumar, G. Mago, V. Balan and C. E. Wyman, *Bioresour Technol*, 2009, **100**, 3948-3962.

33. A.-I. Yeh, Y.-C. Huang and S. H. Chen, *Carbohydrate Polymers*, 2010, **79**, 192-199.

34. A. P. Sinitsyn, A. V. Gusakov and E. Y. Vlasenko, *Applied Biochemistry and Biotechnology*, 1991, **30**, 43-59.

35. J. S. Luterbacher, J. Y. Parlange and L. P. Walker, *Biotechnol Bioeng*, 2013, **110**, 127-136.

36. T. Jeoh, C. I. Ishizawa, M. F. Davis, M. E. Himmel, W. S. Adney and D. K. Johnson, *Biotechnol Bioeng*, 2007, **98**, 112-122.

37. V. P. Puri, *Biotechnology and Bioengineering*, 1984, **26**, 1219-1222.

38. H. Zhao, J. H. Kwak, Y. Wang, J. A. Franz, J. M. White and J. E. Holladay, *Energy & Fuels*, 2006, **20**, 807-811.

39. H. Zhao, J. Kwak, Z. Conradzhang, H. Brown, B. Arey and J. Holladay, *Carbohydrate Polymers*, 2007, **68**, 235-241.

40. L. T. Fan, Y. H. Lee and D. H. Beardmore, *Biotechnology and Bioengineering*, 1980, **22**, 177-199.

41. P. Calvini, A. Gorassini and A. L. Merlani, *Cellulose*, 2007, **15**, 193-203.

42. M. Möller, F. Harnisch and U. Schröder, *RSC Advances*, 2013, **3**.

43. Y. Yu and H. Wu, *AIChE Journal*, 2011, **57**, 793-800.

44. P. Phanthong, G. Guan, Y. Ma, X. Hao and A. Abudula, *Journal of the Taiwan Institute of Chemical Engineers*, 2016, **60**, 617-622.

45. H. J. Philipp, M. L. Nelson and H. M. Ziifle, *Textile Research Journal*, 1947, **17**, 585-596.

46. O. A. Battista, *Industrial & Engineering Chemistry*, 1950, **42**, 502-507.

47. S. Park, J. O. Baker, M. E. Himmel, P. A. Parilla and D. K. Johnson, *Biotechnology for Biofuels*, 2010, **3**, 10.

48. A. P. Dadi, S. Varanasi and C. A. Schall, *Biotechnol Bioeng*, 2006, **95**, 904-910.

49. J. Zhang, B. Zhang, J. Zhang, L. Lin, S. Liu and P. Ouyang, *Biotechnol Adv*, 2010, **28**, 613-619.

50. Q. Zhang, M. Benoit, K. De Oliveira Vigier, J. Barrault, G. Jégou, M. Philippe and F. Jérôme, *Green Chemistry*, 2013, **15**.

51. M. Foston and A. J. Ragauskas, *Biomass and Bioenergy*, 2010, **34**, 1885-1895.

52. F. Hu and A. Ragauskas, *BioEnergy Research*, 2012, **5**, 1043-1066.

53. P. H. Hermans and A. Weidinger, *Journal of the American Chemical Society*, 1946, **68**, 1138-1138.

54. J. A. Howsmon and R. H. Marchessault, *Journal of Applied Polymer Science*, 1959, **1**, 313-322.

55. I. L. Wadehra and R. S. J. Manley, *Journal of Applied Polymer Science*, 1965, **9**, 2627-2630.

56. D. F. Caulfield and R. A. Steffes, *TAPPI*, 1969, **52**, 1361-1366.

57. H. Hatakeyama and T. Hatakeyama, *Makromol Chem*, 1981, **182**, 1655-1668.

58. M. Kimura, Hatakeya.T and J. Nakano, *Journal of Applied Polymer Science*, 1974, **18**, 3069-3076.

59. P. Wormald, K. Wickholm, P. T. Larsson and T. Iversen, *Cellulose*, 1996, **3**, 141-152.

60. S. Ouajai and R. A. Shanks, *Cellulose*, 2006, **13**, 31-44.

61. U. P. Agarwal, S. A. Ralph, C. Baez, R. S. Reiner and S. P. Verrill, *Cellulose*, 2017, **24**, 1971-1984.

62. D. A. Cantero, M. D. Bermejo and M. J. Cocero, *The Journal of Supercritical Fluids*, 2013, **75**, 48-57.

63. M. J. Taherzadeh and K. Karimi, *Int J Mol Sci*, 2008, **9**, 1621-1651.

64. P. Bansal, M. Hall, M. J. Realff, J. H. Lee and A. S. Bommarius, *Bioresour Technol*, 2010, **101**, 4461-4471.

65. D. M. Mowery, D. J. Harris and K. Schmidt-Rohr, *Macromolecules*, 2006, **39**, 2856-2865.

66. L. Segal, J. J. Creely, A. E. Martin and C. M. Conrad, *Textile Research Journal*, 1959, **29**, 786-794.

67. R. L. Johnson and K. Schmidt-Rohr, *J Magn Reson*, 2014, **239**, 44-49.

68. P. Duan and K. Schmidt-Rohr, *J Magn Reson*, 2017, **285**, 68-78.

69. E. L. Hahn, *Physical Review*, 1950, **80**, 580-594.

70. G. Bodenhausen, R. Freeman and D. L. Turner, *Journal*, **27**, 511-514-511-514.

71. B. M. Fung, A. K. Khitrin and K. Ermolaev, *J Magn Reson*, 2000, **142**, 97-101.

72. D. A. Torchia, *Journal of Magnetic Resonance (1969)*, 1978, **30**, 613-616.

73. D. D. Y. Ryu, S. B. Lee, T. Tassinari and C. Macy, *Biotechnology and Bioengineering*, 1982, **24**, 1047-1067.

74. S. E. Jacobsen and C. E. Wyman, in *Twenty-First Symposium on Biotechnology for Fuels and Chemicals: Proceedings of the Twenty-First Symposium on Biotechnology for Fuels and Chemicals. Applied Biochemistry and Biotechnology.*, eds. M. Finkelstein and B. H. Davison, Humana Press, Totowa, NJ, 2000, DOI: 10.1007/978-1-4612-1392-5_6, pp. 81-96.

75. M. L. Nelson, *Journal of Polymer Science*, 1960, **43**, 351-371.

76. P. Bansal, M. Hall, M. J. Realff, J. H. Lee and A. S. Bommarius, *Biotechnol Adv*, 2009, **27**, 833-848.

77. A. C. O'Sullivan, *Cellulose*, 1997, **4**, 173-207.

78. Z. Ling, T. Wang, M. Makarem, M. Santiago Cintrón, H. N. Cheng, X. Kang, M. Bacher, A. Potthast, T. Rosenau, H. King, C. D. Delhom, S. Nam, J. Vincent Edwards, S. H. Kim, F. Xu and A. D. French, *Cellulose*, 2019, **26**, 305-328.

79. C. Driemeier and G. A. Calligaris, *Journal of Applied Crystallography*, 2011, **44**, 184-192.

80. U. P. Agarwal, R. S. Reiner and S. A. Ralph, *Cellulose*, 2010, **17**, 721-733.

81. M. L. Nelson and R. T. O'Connor, *Journal of Applied Polymer Science*, 1964, **8**, 1325-1341.

82. U. P. Agarwal, S. A. Ralph, R. S. Reiner and C. Baez, *Cellulose*, 2015, **23**, 125-144.

83. R. H. Newman, *Cellulose*, 2004, **11**, 45-52.

84. J. H. Wiley and R. H. Atalla, *Carbohyd Res*, 1987, **160**, 113-129.

85. R. H. Newman and T. C. Davidson, *Cellulose*, 2004, **11**, 23-32.

86. P. Bhama Iyer, S. Sreenivasan, P. K. Chidambareswaran and N. B. Patil, *Textile Research Journal*, 1984, **54**, 732-735.

87. B. F. Wood, A. H. Conner and C. G. Hill, *Journal of Applied Polymer Science*, 1989, **37**, 1373-1394.

88. M. Ioelovich, A. Leykin and O. Figovsky, *Bioresources*, 2010, **5**, 1393-1407.

89. S. Nam, A. D. French, B. D. Condon and M. Concha, *Carbohydr Polym*, 2016, **135**, 1-9.

90. M. Akerholm, B. Hinterstoisser and L. Salmen, *Carbohydr Res*, 2004, **339**, 569-578.

91. J.-H. Lin, Y.-H. Chang and Y.-H. Hsu, *Food Hydrocolloids*, 2009, **23**, 1548-1553.

92. R. N. Ibbett, D. Domvoglou and D. A. S. Phillips, *Cellulose*, 2007, **15**, 241-254.

93. L. T. Fan, M. M. Gharpuray and Y. H. Lee, *Cellulose hydrolysis. Biotechnology monographs. Volume 3*, Springer-Verlag,New York, NY; None, 1987.

94. F.-X. Collard and J. Blin, *Renewable and Sustainable Energy Reviews*, 2014, **38**, 594-608.

95. C. M. Cai, T. Zhang, R. Kumar and C. E. Wyman, *Green Chemistry*, 2013, **15**.